Theoretical Study of Particle Dissolution during Homogenization in Cu–Fe–P Alloy

Spyros Papaefthymiou [1],* iD **, Marianthi Bouzouni [1,2] and Evangelos Gavalas [1,2]** iD

[1] Laboratory of Physical Metallurgy, Division of Metallurgy and Materials, School of Mining & Metallurgical Engineering, National Technical University of Athens, 9, Her. Polytechniou str., Zografos, 15780 Athens, Greece; mbouzouni@elkeme.vionet.gr (M.B.); egavalas@elkeme.vionet.gr (E.G.)

[2] Department of Physical Metallurgy and Forming, Hellenic Research Centre for Metals S.A.—ELKEME S.A., 56th km Athens-Lamia Nat. Road, 32011 Oinofyta, Greece

* Correspondence: spapaef@metal.ntua.gr; Tel.: +30-210-772-4710

check for updates

Abstract: The effect of temperature, soaking time and particle size on the dissolution of particles (Fe$_3$P and Fe) during homogenization was simulated employing Thermocalc® and DICTRA software. The initial precipitate size was determined through metallographic evaluation on industrial as-cast Cu–Fe–P alloy. The particle sizes vary from submicron (<1 μm) up to 10 μm before the heat treatment. As homogenization temperature rises, the dissolution rate increases as well, but only on temperatures above 1273 K (1000 °C) is the rate capable of completely dissolving particles effectively. At temperatures above 1273 K (1000 °C), precipitates with sizes below 5 μm dissolve completely into the Cu matrix, while larger particles only slightly decrease their size. Particles at enriched copper areas remain undissolved and slightly increase their size which is attributed to micro segregation and the local change of equilibrium conditions. The simulation results are in agreement with homogenization trials at lab scale.

Keywords: Cu–Fe–P; dissolution; diffusion; homogenization; heat treatment; Fe$_3$P; Fe particles; solid solution

1. Introduction

The increased requirements for economic copper (Cu) tubes being able to withstand higher pressures while working in extreme service environments and maintain their conductivity have led to research around a number of Cu-based alloys with higher mechanical properties. The endeavor to increase the mechanical properties of solid solution hardened alloys is limited by their insufficient relaxation resistance at slightly increased temperatures and decreasing electrical and thermal conductivity when heavily alloyed. To overcome this, the focus has turned to precipitation-hardened alloys [1,2]. Recently, copper–iron–phosphorus (Cu–Fe–P) alloys have been a successful medium-strength and high-conductivity alternative that provide superior properties over other widely used materials for copper tubes, such as deoxidized-high-phosphorus (DHP) copper [3].

The industrial application and the effects of thermomechanical processing on the microstructure and second-phase particles have been studied in [4–6]. The improvement of the mechanical properties in Cu–Fe–P alloys is attributed to precipitation hardening via fine dispersion of particles (α-Fe, γ-Fe, Fe$_3$P) in the Cu matrix and the materials' resistance to softening due to recrystallization [2,4,5,7,8].

In Cu–Fe–P alloys, small-sized particles (submicron scale), found at the grain boundaries, are desirable in the microstructure as they control recrystallization and pin grain boundaries and dislocations via the Zener drag mechanism [4,5,9], thereby limiting grain growth. Coarse particles should be avoided as they do not pin dislocations and grain boundaries during recrystallization which

results in reduced mechanical properties and material sensitivity at high temperatures. Homogeneous distribution of fine particles is of great importance and is achieved via appropriate precipitation heat treatment, which consists of homogenization, quenching and aging. During homogenization, the temperature must be high enough to induce the dissolution of particles. This procedure is followed by quenching in which the cooling rate must prevent any diffusion and precipitation, and ensure that the copper (Cu) matrix is supersaturated with phosphorous (P) and iron (Fe) atoms. Finally, during the aging treatment the required driving force is provided for the supersaturated matrix to reach equilibrium. So, fine particles begin to form homogeneously. The size of phosphides depends on the temperature and time for aging and not on the final cooling rate [10].

Since the properties of Cu–Fe–P alloys are greatly influenced by microalloying, each production step has to be carefully designed to achieve the required final properties. Many researchers have applied various methods to optimize mechanical and material (i.e., thermal conductivity, microstructure, etc.) properties. Extensive investigation has been held on the influence of various alloying elements (e.g., Ni, Si, Mg, Mn) and their concentration on the Cu matrix [6,11–15]. Lu et al. [11] showed that traces of boron B and cerium Ce could increase the recrystallization temperature, succeeding more complete aging and, thus, obtaining the strengthening effect via work and precipitation hardening. Brovč et al. [12] and Yamamoto et al. [13,14] indicated the high potential of Cu–Fe–Ni–P alloy, illustrating the good conductivity and mechanical properties at elevated temperatures, as an alternative economic alloy, in order to avoid the addition of toxic (i.e., Cd, Be) or precious metals (e.g., Ag) used until now as alloying elements in the industry. The addition of Mg, Si, Pb and Mn further improve the mechanical properties of the alloy without compromising conductivity when carefully used [6,15].

Since the results of annealing at the final stages of copper tube production, where recrystallization and aging takes place, have as a prerequisite an efficient homogenization at the beginning of the production process, the dissolution of Fe and Fe_3P particles during homogenization is of great importance. Particle dissolution theory initially introduced by Whelan [16], describes the solute flux in conjunction with the particle size and concentrations. The diffusional growth and dissolution has been studied extensively in terms of interface movement and diffusion of solute atoms in iron systems [17–19]. However, little work has been done on non-ferrous alloys.

Although both the alloying and the ageing treatment have been thoroughly studied, the homogenization step has not been adequately investigated. Several homogenization strategies have been implemented industrially and many researchers have analyzed the effect of temperature and time on homogenization annealing, using only material characterization techniques but without explaining the criteria of the optimal homogenization and specifying the optimal conditions for a successful homogenization [4,7,11,12]. Parameters are difficult to be determined and are very important for industrial production, where time and sizes impose limitations.

For this purpose, homogenization experiments were simulated with the aid of Thermocalc® and DICTRA software at various temperatures and soaking times in order to understand the influence of the process conditions and the local chemical composition on the Fe-rich particle dissolution. The results have been compared to experimental data in order to determine the homogenization behavior of Cu–Fe–P alloy.

2. Material and Modelling

The chemical composition of an industrially produced billet with a diameter of 600 mm is shown in Table 1, which complies with BS EN 12449:2012 standard [20]. The Thermocalc® (Version 2018a, Thermo-Calc Software AB, Solna, Sweden) calculation of the alloy's phase diagram, utilizing the CALculation of PHAse Diagrams—CALPHAD method, has been deployed in order to predict the phases formed in crucial temperature areas and determine the temperature window for the homogenization process. Through metallographic evaluation, the different sizes of precipitates were measured and used as input data for the simulation. For the simulation of homogenization, three phases

were considered: Fe, Fe$_3$P and Cu matrix. The system was limited to Cu–Fe–P–Zn. The alloy's solidification was simulated in DICTRA (Version 2018a, Thermo-Calc Software AB, Solna, Sweden) with a cooling rate 10 K/s in order to predict the chemical composition of the Cu matrix (Table 2).

Table 1. Alloy's composition.

Fe (%)	P (%)	Zn (%)	Cu (%)
2.3	0.025	0.12	97.555

Table 2. Composition of Cu matrix in alloying element-depleted regions.

Fe (%)	P (%)	Zn (%)
1.8	0.01	0.1291

The activation enthalpies were set at 250,000 J/mol and 210,000 J/mol respectively determined by Thermocalc. Similar values for the activation enthalpy can be found elsewhere [21].

The effect of segregation upon homogenization was taken into account in this study as it greatly affects the homogenization result. Thus, additional simulations were carried out for particles dissolving in an alloying element-enriched Cu matrix whose chemical composition is shown in Table 3. The chemical composition was defined by Thermocalc® considering that the segregated zones obtain the chemical composition of the Cu matrix at the beginning of the solidification, as given in Table 3.

Table 3. Composition of Cu matrix in alloying element-enriched regions.

Fe (%)	P (%)	Zn (%)
3.8	0.025	0.15

In Figure 1 the particle distribution in the initial microstructure before homogenization is illustrated. The particles are spherical or quasi-spherical, thus the system has been modeled with spherical particle of predefined size (D_p) surrounded by copper matrix with a radius of 100 μm, as depicted in Figure 2. The radius of the matrix refers to the sample's average grain size; however, the influenced area was studied in order to ensure that there is no interaction between two neighboring particles of the same size. The initial particle size of Fe$_3$P particles was selected to be 1, 5, 7 and 10 μm and of the Fe particles 1 μm with spherical geometry, respectively, based on metallographic results.
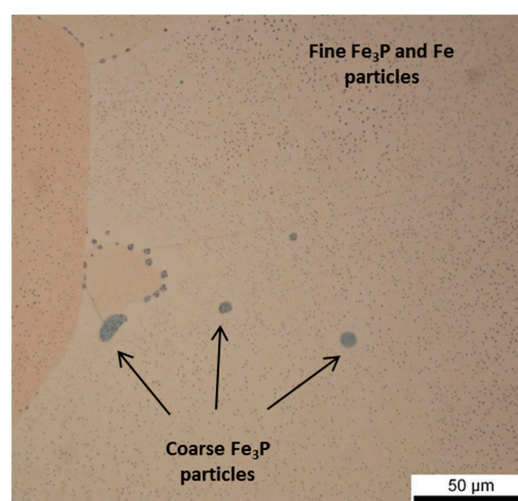

Figure 1. Microstructure of Cu–Fe–P alloy. Fe$_3$P particles appear with size ranging from 1–10 μm preferably at grain boundaries whereas Fe particles are homogeneously distributed in the Cu matrix.
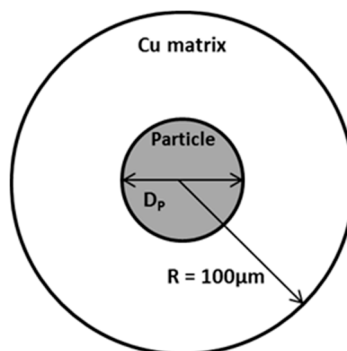
Figure 2. Schematic representation of the system used for DICTRA calculations. The D_P obtains values 1 μm, 5 μm, 7 μm, 10 μm.

Two sets of simulations for each individual particle were held at the following temperatures: 1073 K (800 °C), 1173 (900 °C) and 1273 K (1000 °C). In the first set, particle dissolution took place in the alloying element-depleted Cu matrix (Table 2), and in the second set dissolution simulations took place in the alloying element-enriched Cu matrix (Table 3). The temperature of 1073 K (800 °C) was defined as the lowest temperature that the billet can be extruded in an industrial extrusion press. The maximum soaking time selected for the homogenization simulations was 10 h. The heating rate used to reach the homogenization temperature was 1 K/s. An estimate of the mobility expression [21] of Fe and P for the Fe$_3$P and Fe particle was made,

$$M = \frac{M^o}{RT} \exp\left(\frac{-Q}{RT} \right) \tag{1}$$

in which $M°$ is the frequency factor, Q the activation enthalpy, R is the constant for gas and T is the temperature. Calculations were performed using DICTRA software and the databases TCCU1 and MOBCU1 assuming that local equilibrium exists at interfaces [22].

3. Modelling Results

3.1. Phase Diagram

The calculated isopleth sections of phase diagrams of the Cu–Fe–P alloy in thermodynamic equilibrium are illustrated in Figures 3 and 4. The diagrams show that the phases that exist at equilibrium are liquid, Cu (matrix), γ-Fe, α-Fe and Fe$_3$P while the red lines denote the examined alloy's chemical composition also indicated in Table 1. Fe$_3$P and α-Fe precipitates form in temperatures below 973–1230 K (700–957 °C) depending on the local chemical composition. The influence of the Fe and P on the phase diagram has been studied as well in order to understand the influence of local chemical composition variation. By increasing Fe concentration, the Fe$_3$P dissolution threshold temperature slightly decreases by ~30 K in the range from 2.1% Fe to 2.6% Fe, as shown in Figure 3. However, P plays a more important role as depicted in Figure 4. By increasing P concentration from 0.015% P to 0.05% P, the Fe$_3$P dissolution temperature increases from 843 K (570 °C) to 1033 K (760 °C). The liquid temperature is not influenced by chemical composition variation of Fe and P.
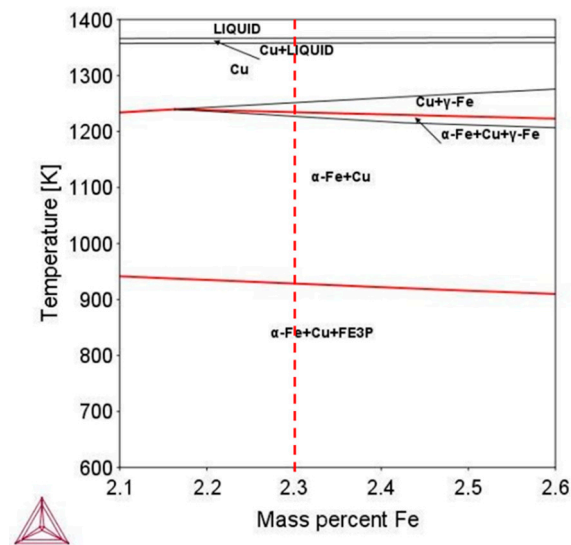
Figure 3. Isopleth section of CuFe$_2$P alloy phase diagram—Fe dependency. The red lines show the temperatures at which α-Fe and Fe$_3$P particles are formed depending on Fe content.
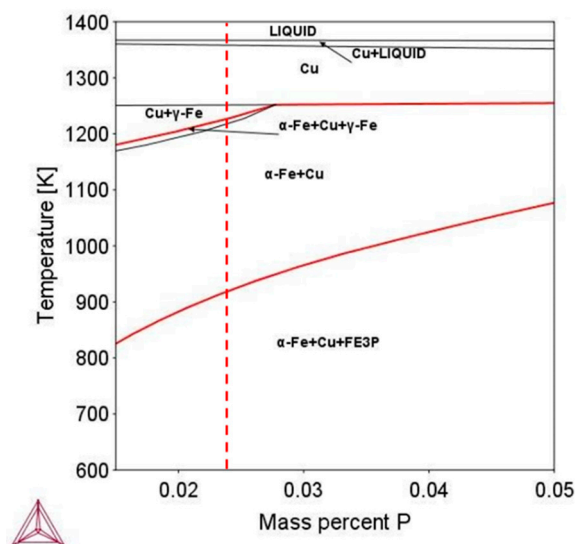

Figure 4. Isopleth section of CuFe$_2$P alloy phase diagram—P dependency. The red lines show the temperatures at which α-Fe and Fe$_3$P particles are formed depending on P content.

3.2. Dissolution Calculations

In Figures 5–7 the particle size evolution during homogenization, in both alloying element depleted and enriched regions, is illustrated for various initial particle diameters and different soaking temperatures.

At 1073 K (800 °C) the graphs remain almost parallel to the abscissa axis at the depleted matrix simulations. According to the phase diagrams (Figures 3 and 4), although it is thermodynamically feasible to perform homogenization at the temperature of 1073 K (800 °C), since it is higher than the dissolution threshold temperature, practically there is no phosphide size alteration for the given time. The low temperature limits the diffusion rate which in turn deteriorates the particle dissolution (Figure 5).
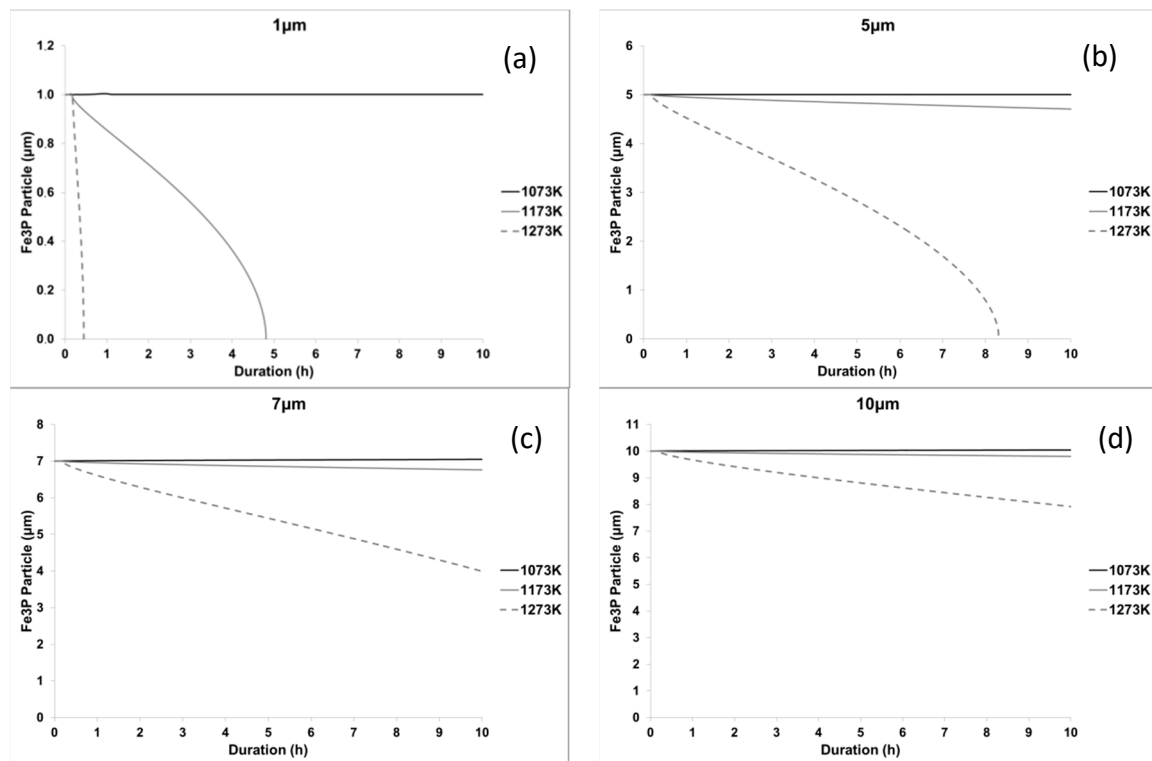
Figure 5. Simulation results of homogenization of Fe₃P particles in the Cu matrix tested at various temperatures for (**a**) 1 μm, (**b**) 5 μm, (**c**) 7 μm, (**d**) 10 μm.
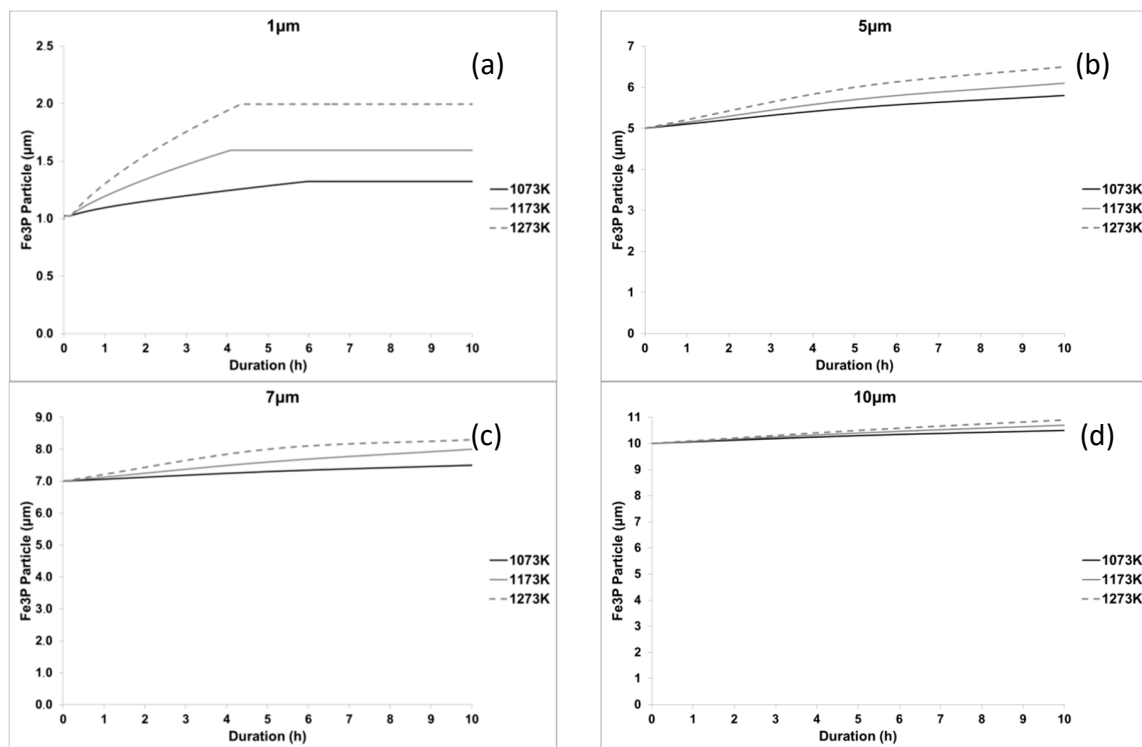

Figure 6. Simulation results of homogenization of Fe₃P particles in an enriched Cu matrix tested at various temperatures for (**a**) 1 μm, (**b**) 5 μm, (**c**) 7 μm, (**d**) 10 μm.
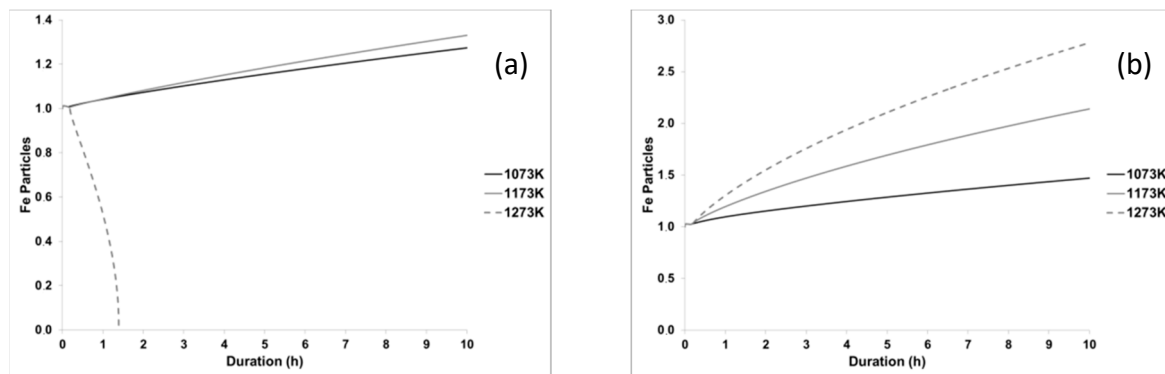
Figure 7. Simulation results of homogenization for Fe particles tested at various temperatures for (**a**) depleted copper matrix in Fe and P (**b**) enriched copper matrix in Fe and P.

By increasing the temperature, the diffusion rate increases as well for all particle sizes. Complete dissolution of small size Fe_3P particles (1 µm) is evident from the temperature of 1173 K (900 °C) within the experimental homogenization duration (Figure 5a). However, particle size influences the dissolution rate notably. Fe_3P particles with initial size of 5 µm could not dissolve in temperatures below 1173 K (900 °C) (Figure 5b), while Fe_3P particles with 7 µm initial size require even higher temperature ~1223 K (~950 °C) (Figure 5c). Large Fe_3P particles (10 µm) do not dissolve even at 1273 K (1000 °C) within the 10 h soaking time (Figure 5d).

The homogenization duration time is also an important factor. Small size particles (1 µm) require from almost 10 h at temperature of 1073 K (800 °C) to only few minutes as the temperature rises to 1273 K (1000 °C) (Figures 5a and 7a). The larger particles (7 µm, 10 µm), although undissolved, slightly reduce their size by increasing temperature until 1273 K (1000 °C) (Figure 5c,d).

The surrounding copper matrix also significantly affects the particle dissolution. In regions enriched in alloying elements, the particles not only remain undissolved but increase their size (Figures 6 and 7) as the copper matrix is supersaturated.

As a particle dissolves, the surrounding area is enriched in alloying elements. The influenced area around a dissolving particle is smaller than half of the distance between two neighboring particles of the same size, which indicates that there is no interaction between them. A representative illustration of the influenced area can be seen in Figure 8. The Fe concentration of the surrounding region of a dissolving 1 µm (R = 0.5 µm) particle, exactly the moment that complete dissolution is realized, suggests that the Fe concentration reaches the nominal concentration of the Cu matrix only 2.5 µm away from the initial position of the particle–matrix interface.
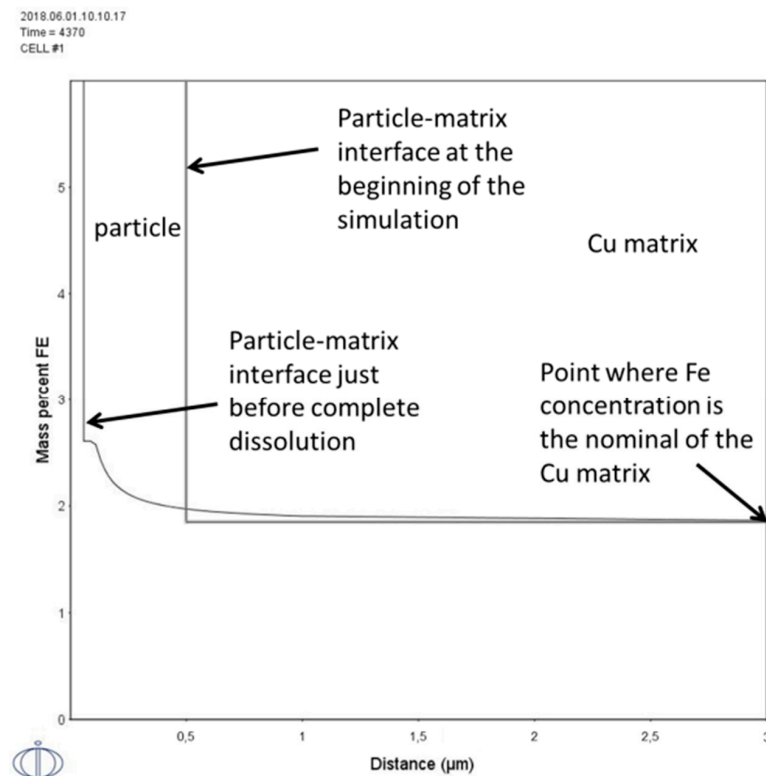
Figure 8. Fe concentration around a 1 μm (*R* = 0.5 μm) particle at the beginning and the end of the dissolution process.

4. Homogenization Trials

Specimens from the center of an industrially produced billet, with a diameter of 600 mm, were obtained and homogenized at 1273 K (1000 °C) for 10 h and then water quenched. The metallographic evaluations, illustrated in Figure 9, are in good correlation with the simulation results. A significant number of small particles (~1 μm) were dissolved whereas elliptical Fe particles with increased size and coarse spherical Fe_3P particles were apparent in the microstructure. Scanning electron microscopy–energy dispersive X-ray spectroscopy (SEM–EDS) (Philips XL40 sfeg, Amsterdam, Netherlands) analysis indicates that the spherical particles are Fe_3P particles since the Fe/P analogy is ~3 whereas the elliptical/rod like particles are Fe particles (Figure 10).
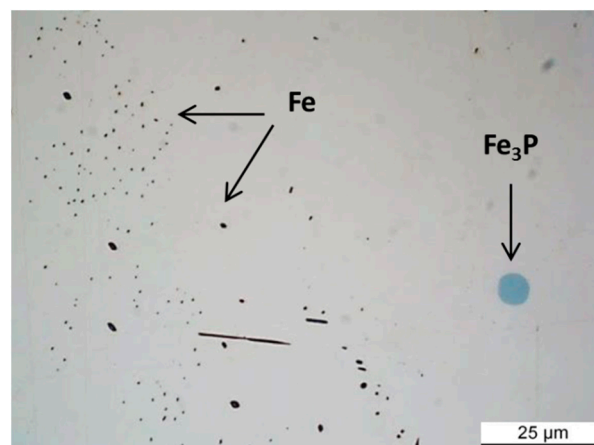

Figure 9. Microstructure of Cu–Fe–P alloy after homogenization. The majority of submicron particles are dissolved. Coarse Fe_3P particles remain undissolved while Fe particles with increased size appear.
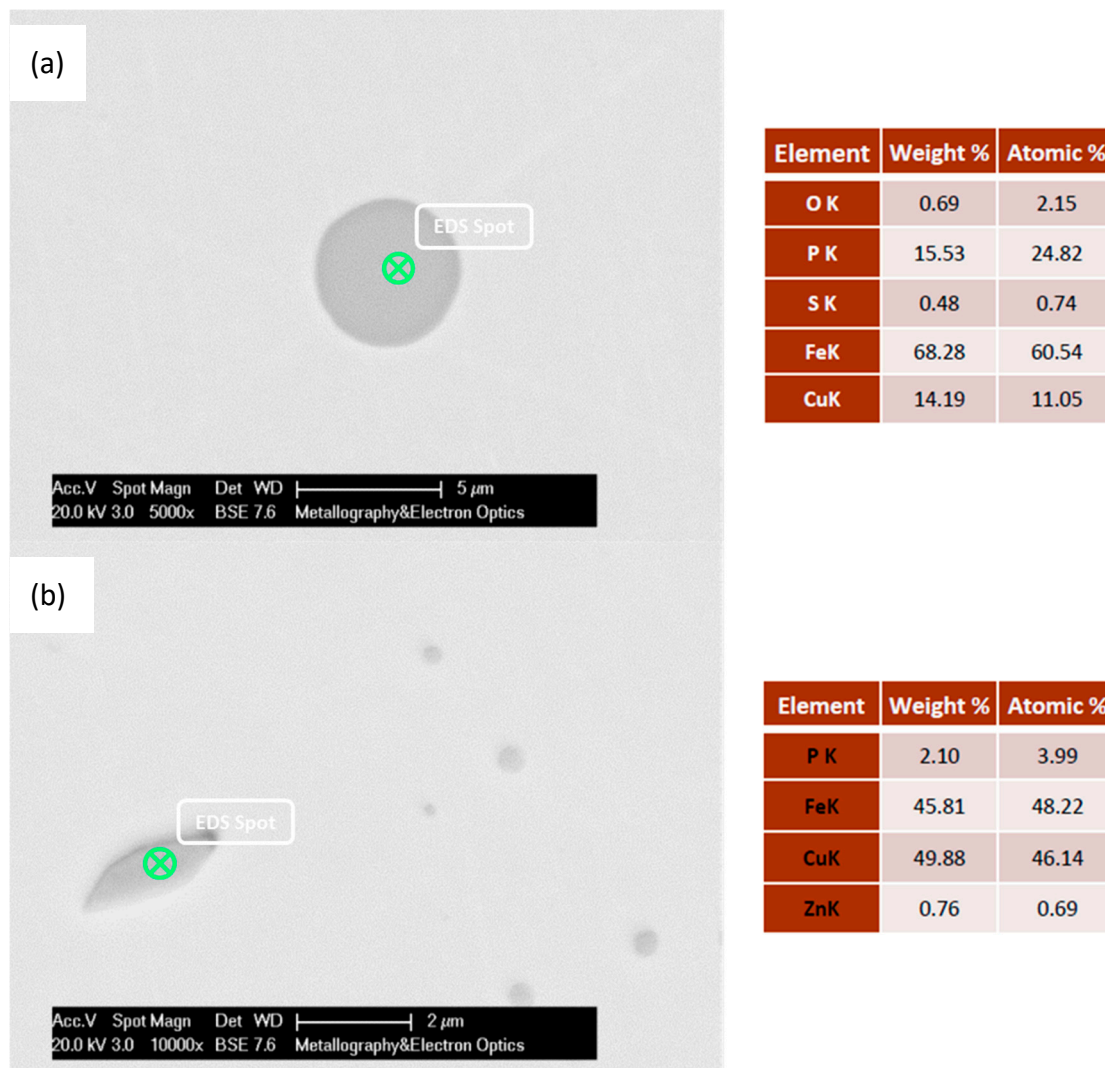
Element	Weight %	Atomic %
O K	0.69	2.15
P K	15.53	24.82
S K	0.48	0.74
FeK	68.28	60.54
CuK	14.19	11.05

Element	Weight %	Atomic %
P K	2.10	3.99
FeK	45.81	48.22
CuK	49.88	46.14
ZnK	0.76	0.69

Figure 10. Scanning electron microscopy–energy dispersive X-ray spectroscopy (SEM–EDS) analysis on the intermetallic particles (**a**) spherical Fe$_3$P particle, (**b**) elliptical Fe enriched particle. The arrow indicates where the chemical analysis was taken.

5. Discussion

Intermetallic particle size can greatly vary depending on the production conditions of the examined sample. A laboratory specimen is ideally produced in clean conditions with controlled cooling and casting speed. By contrast, in industrially produced billets due to centerline segregation and slow cooling rates the amount of larger-sized particles found in the billet's center is increased and, consequently, this is the most insensitive area during the homogenization process in terms of particle dissolution. This causes inhomogeneity across the billet's thickness. A different thermodynamic equilibrium applies to the center of the billet compared to conditions at the outer surface due to different alloying element concentration (Figure 4). An important criterion for the decision of homogenization temperature and time is the initial microstructure of the processed sample.

The process window for an industrially produced billet lies in the high temperature range for 1.5–2 h. From the results it can be observed that mainly the small particles in high temperature simulations were dissolved, requiring less than two hours for this purpose. Any further time results in no further dissolution and in some cases in particle growth, possible defects and additional production cost. A homogenization anneal at the low-temperature range will have almost no effect on the material.

The duration of homogenization can vary from a few minutes to many hours even for small-sized particles (1–5 µm) at temperatures in which Fe_3P particles should have been dissolved (~800 °C) according to the phase diagram. Since the Cu matrix is not in equilibrium but filled with alloying elements in solid solution, the diffusion rate decreases, restricting the particle dissolution.

Although small particles were successfully dissolved, large particles were still found in the microstructure after the homogenization, as expected after the simulation. However, it is obvious that there are regions with increased large particle concentration. As can be seen from the phase diagrams (Figures 3 and 4), in the case of P, increased local concentration, due to excessive segregation, dramatically increases the dissolution temperature and stabilizes the phosphide particles making the dissolution even more difficult. Moreover, copper regions enriched in alloying elements are supersaturated and it is difficult for Fe to diffuse and, therefore, it remains in solid solution in the Cu matrix. Figure 11 shows the concentration profile of Fe at the Fe particle/Cu matrix interface. C_β is the Fe concentration in the Fe particle as expected by equilibrium, whereas C_α is the Fe concentration in Cu matrix at equilibrium. C_o is the Fe content of the supersaturated Cu matrix. When $C_\alpha < C_o$, it means that the Fe content has to reach the C_α composition in the Cu matrix, thus, there is a flux of Fe atoms from the matrix towards the Fe particle and diffusional growth can be achieved. When $C_\alpha > C_o$, this indicates that the Fe content in the Cu matrix should reach C_α composition. In order to achieve this, Fe atoms diffuse from the Fe particle towards Cu matrix and the dissolution of Fe particles can be achieved. The different solubility of particles and Cu matrix is attributed to the chemical composition and crystal structure. Fe_3P and Fe particles were considered to have a BCC (body centered cubic) structure whereas the Cu matrix has an FCC (face centered cubic) structure. The flux of solute atoms towards the interface is described by an error function introduced by Whelan [16]. The diffusional distance that the atoms have to move Δx can be calculated from, the overall concentration of mass is given by Equation (2) for isothermal transformation [23]:

$$(C_\beta - C_o)x = \frac{1}{2}(C_o - C_a)\Delta x \qquad (2)$$

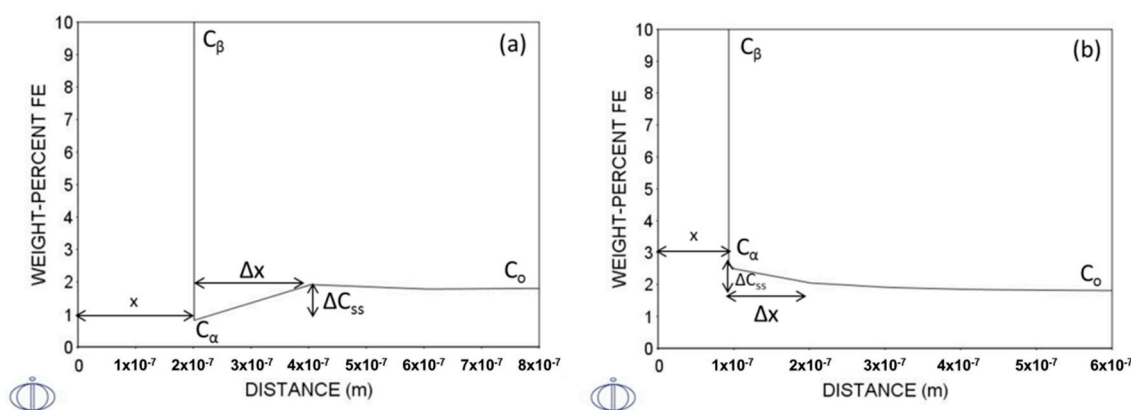where C stands for concentration and x for particle size.

Figure 11. Plot of Fe profiles versus Cu matrix (**a**) growth of Fe particles, (**b**) dissolution of Fe particles. The diagrams are concentrated on the interface thus C_β is 90 wt. %.

It can be observed that in alloying element-enriched regions, particles had even increased their size. The increase of particle size can also be explained from the Ostwald ripening theory where large particles are more energetically stable than smaller particles. Atoms of the small particles diffuse and attach to the large particles resulting in large particles growing in size and small particles shrinking [24].

6. Conclusions

Particle dissolution has been investigated during the homogenization process in a Cu–Fe–P alloy via Thermocalc® and DICTRA software. The phase diagrams indicate that the iron mass percentage does not influence the dissolution temperature. However, higher phosphorus concentration stabilizes the Fe_3P loop and increases the dissolution temperature. According to the simulation results, the particle dissolution depends on four critical parameters influencing each other: (a) the size of phosphides; (b) soaking time; (c) the temperature of homogenization; and (d) the local chemical composition of the base metal. In alloying element-depleted regions dissolution was realized in approximately 1 h for the small particles of 1 μm in the temperature of 1273 K (1000 °C). Larger particles are more difficult, requiring longer, or are even impossible to dissolve. Chemical heterogeneity due to segregation caused local phenomena of a higher element concentration in the base metal, resulting in particles either remaining undissolved or in many cases increasing in size due to the Ostwald ripening phenomena. Metallographic evaluation showed that the experiments are consistent with the simulation. Microsegregation is evident in the initial microstructure situated mainly in grain boundaries and interdendritic regions. The homogenization heat treatment created in the microstructure patches of precipitation-free regions and other regions with a small number of enlarged particles due to a different local chemical equilibrium.

For the optimal homogenization of the specific material, a high temperature of 1273 K (1000 °C) is required. Homogenization time of 1.5–2 h will result in the dissolution of the small particles without affecting the larger ones. Longer soaking time will result in no further dissolution.

Author Contributions: Conceptualization, S.P.; Methodology, S.P., E.G. and M.B.; Validation, E.G., M.B. and S.P.; Writing–Original Draft Preparation, M.B.; Writing–Review and Editing, S.P. & E.G.; Supervision, S.P.; Project Administration, E.G.

References

1. Pawlek, F.; Reichel, K. Der Einfluss von Beimengungen auf die elektrische Leitfähigkeit von Kupfer. *Z. Met.* **1956**, *47*, 347–356.

2. Zauter, R.; Kudashov, D.V. Precipitation hardened high copper alloys for connector pins made of wire. In Proceedings of the 23rd International Conference on Electrical Contacts ICEC2006/Sendai, Sendai, Japan, 6–9 June 2006.

3. Pantazopoulos, G.; Toulfatzis, A.; Zormalia, S.; Vazdirvanidis, A.; Skarmoutsos, D. Preliminary evaluation of the thermally affected metallurgical condition of extruded and drawn $CuFe_2P$ tubes. *J. Mater. Eng. Perform.* **2012**, *21*, 2188–2194. [CrossRef]

4. Dong, Q.-Y.; Shen, L.-N.; Wang, M.-P.; Jia, Y.-L.; Li, Z.; Cao, F.; Chen, C. Microstructure and properties of Cu−2.3Fe−0.03P alloy during thermomechanical treatments. *Trans. Nonferrous Metals Soc. China* **2015**, *25*, 1551–1558. [CrossRef]

5. Cao, H.; Min, J.Y.; Wu, S.D.; Xian, A.P.; Shang, J.K. Re-precipitation of coherent γ-Fe particles following annealing of equal channel angular pressed Cu–Fe alloy. *Mater. Sci. Eng. A* **2006**, *431*, 86–91. [CrossRef]

6. Taro, K.; Motohisa, M.; Kenjyu, M.; Mitsuhiro, O.; Ryoichi, O.; Akinori, T. Corrosion resistant copper alloy tube and fin-tube heat exchanger. European Patent 0626459A1, 27 May 1994.

7. Kim, H.G.; Han, S.Z.; Euh, K.; Lim, S.H. Effects of C addition and thermo-mechanical treatments on microstructures and properties of Cu–Fe–P alloys. *Mater. Sci. Eng. A* **2011**, *530*, 652–658. [CrossRef]

8. Ammannati, N. Method for the production of alloy pipes for heat exchangers using precipitation hardening through underwater extrusion. EP 2027947B1 European Patent Specification, 6 April 2011.

9. Smith, S.C. Grains, phases, and interfaces: An interpretation of microstructure. *Metall. Mater. Trans. B* **1948**, *175*, 15–51.

10. Callister, W.D., Jr.; David, G.R. *Materials Science and Engineering*, 9th ed.; Wiley: Hoboken, NJ, USA, 2014.

11. Lu, D.P.; Wang, J.; Zeng, W.J.; Liu, Y.; Lu, L.; Sun, B.D. Study on high-strength and high-conductivity Cu–Fe–P alloys. *Mater. Sci. Eng. A* **2006**, *421*, 254–259. [CrossRef]

12. Brovc, G.; Drazic, G.; Karpe, B.; Djordjevic, I.; Lojen, G.; Kosec, B.; Bizjak, M. Synthesis and characterization of hardened Cu-Fe-Ni-P alloy. *Metalurgija* **2015**, *54*, 51–54.

13. Yanamoto, Y.; Sasaki, G.; Yamakawa, K.; Ota, M. *Tokio: Hitachi Cable Review*; No. 19; The Technical Journal of Hitachi Cable: Tokyo, Japan, 2000.

14. Yamamoto, Y.; Takano, H.; Ohta, M.; Tong, C.; Kunishige, A. *Tokio: Hitachi Cable Review*; No. 26; The Technical Journal of Hitachi Cable: Tokyo, Japan, 2007.

15. Ohashi, Y.; Fujino, T.; Taki, Y.; Nishijima, T. Aged Copper Alloy with Iron and Phosphorous. U.S. Patent 5,071,494, 10 December 1991.

16. Whelan, M.J. On the kinetics of precipitate dissolution. *Metal Sci. J.* **2013**. [CrossRef]

17. Voice, W.E.; Faulkner, R.G. Computer simulated dissolution of carbide precipitates in alloys. *Metal Sci.* **1984**, *18*, 411–418. [CrossRef]

18. Liu, Z.K.; Höglund, L.; Jönsson, B.; Ågren, J. An experimental and theoretical study of cementite dissolution in an Fe-Cr-C alloy. *Metall. Trans. A* **1991**, *22*. [CrossRef]

19. Liu, Z.K.; Agren, J. Morphology of cementite decomposition in an Fe-Cr-C alloy. *Metall. Trans. A* **1991**, *22*, 1753–1759. [CrossRef]

20. Davis, J.R. Copper and copper alloys—Seamless, round tubes for general purposes. In *BSI Standards Limited 2012: The British Standards Institution*; ASM International: Geauga County, OH, USA, 2012.

21. Butrymowicz, D.B.; Manning, J.R. Michael R. Diffusion in copper and copper alloys. Part III. Diffusion in systems involving elements of the groups IA, IIA, IIIB, IVB, VB, VIB, and VIIB. *J. Phys. Chem. Ref. Data* **1975**. [CrossRef]

22. Borgenstam, A.; Engstrom, A.; Hoglund, L.; Agren, J. Dictra, a tool for simulation of diffusional transformations in alloys. *J. Phase Equilib.* **2000**, *21*, 269–280. [CrossRef]

23. Bhadeshia, H.K.D.H. Course MP6, Kinetics and Microstructure Modelling. Available online: https://www.phase-trans.msm.cam.ac.uk/mphil/MP6-15.pdf (accessed on 13 June 2018).

24. Tada, T.; Seo, T.; Higashimine, K.; Monzen, R. Ostwald ripening of rod-shaped α-Fe particles in a Cu matrix. *Mater. Lett.* **2004**, *58*, 2007–2011.